Soft Matter

www.softmatter.org

Volume 5 | Number 13 | 7 July 2009 | Pages 2481–2668

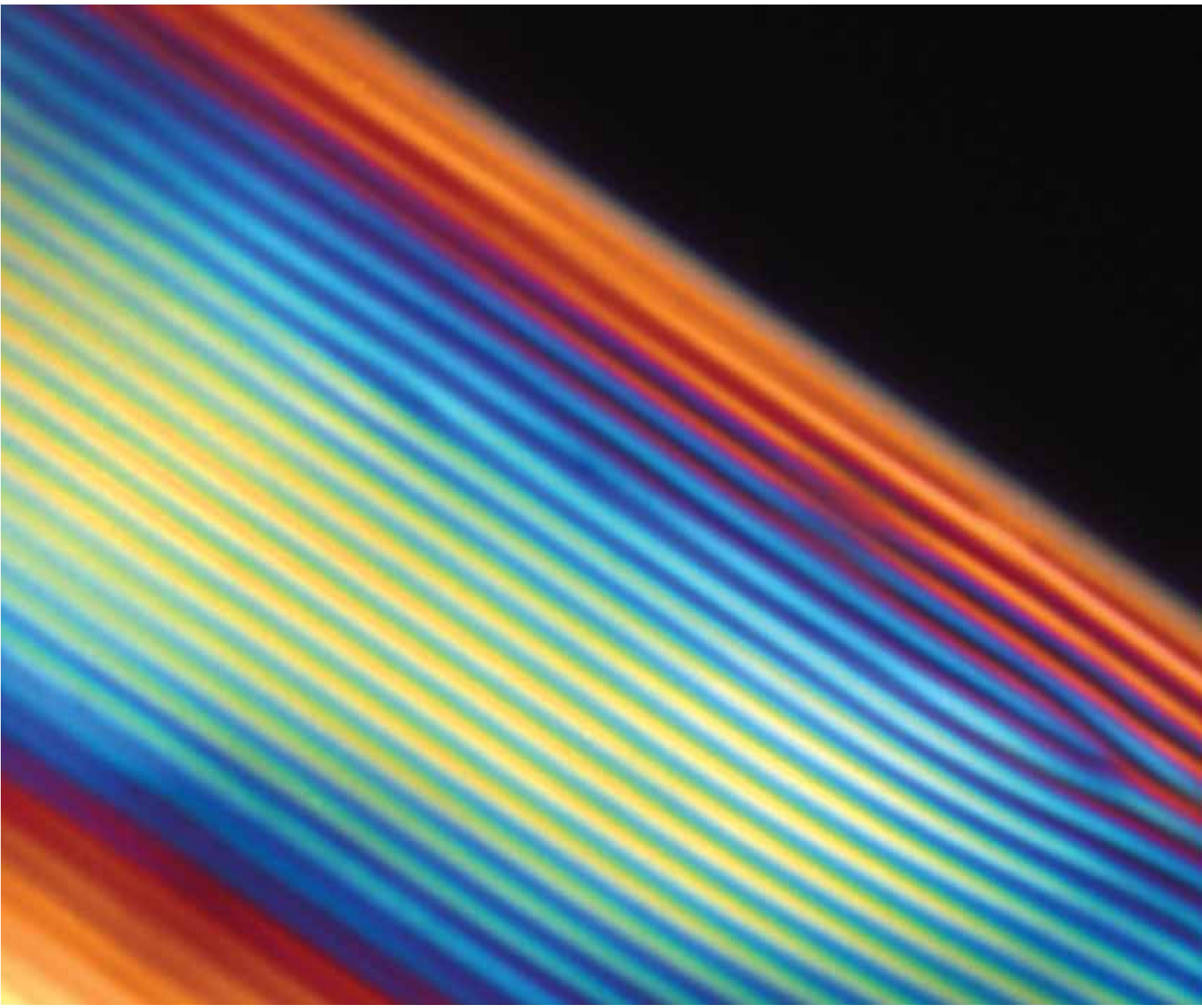

ISSN 1744-683X

RSC Publishing

1744-683X(2009)5:13;1-3

A model liquid crystalline system based on rodlike viruses with variable chirality and persistence length†

Edward Barry, Daniel Beller and Zvonimir Dogic*

Received 16th December 2008, Accepted 25th March 2009
First published as an Advance Article on the web 30th April 2009
DOI: 10.1039/b822478a

We compare the phase behavior of a mutant filamentous virus, *fd* Y21M, to that of a conventional *fd* wild-type (*wt*). We find significantly different macroscopic phase behavior despite the only microscopic difference between the two viruses being in a single amino acid of the major coat protein pVIII. Compared to *fd wt*, the location of the isotropic–cholesteric phase transition for *fd* Y21M shifts to lower densities. This is attributable to a significant difference in the flexibility of the two viruses. The persistence length of *fd wt* is 2.8 ± 0.7 μm, whereas the persistence length of *fd* Y21M is 9.9 ± 1.6 μm. The large persistence length of *fd* Y21M makes it an essentially rigid rod, thus allowing for the first time a quantitative test of the Onsager theory for the isotropic–nematic phase transition. Even more striking, is the difference in the chiral phase behavior of the two viruses. Both viruses form cholesteric phases, with the *fd wt* forming a left-handed cholesteric helix, and the *fd* Y21M forming a right-handed one. At a given density, the magnitude of the cholesteric pitch between the two systems is different by fivefold. Using mixtures of the two viruses, we create a liquid crystalline system with a tunable control over its macroscopic chirality.

1 Introduction

One of the overarching goals in the field of colloidal liquid crystals is to establish a rigorous connection between the macroscopic properties of a liquid crystalline material and the microscopic features of the constituent rodlike molecules such as their aspect ratio, flexibility, and chirality. A seminal milestone in this regard was achieved by Lars Onsager, who over sixty years ago developed a first principles theory for the isotropic–nematic phase transition, demonstrating that hard rods are the simplest system which exhibit a nematic liquid crystalline phase and predicting the exact location of the isotropic–nematic phase transition as a function of rod's aspect ratio and concentration.[1,2] Most realistic particles deviate from the ideal hard rods of the Onsager model, in that they are charge stabilized, have finite flexibility, and are microscopically chiral. To compare the behavior of these particles to theoretical predictions, Onsager theory has to be extended to take these effects into account. Onsager in his original paper showed that a particle's charge primarily acts to increase the effective diameter of rodlike particles. Subsequently, Khokhlov and Semenov (KS) extended the Onsager theory to include the effects of finite rod flexibility, demonstrating that flexibility pushes the isotropic–nematic phase transition to higher densities, reduces the width of the isotropic–nematic coexistence, and lowers the order parameter of the coexisting nematic phase.[3]

Experimentally, one of the most versatile model systems of rodlike particles is based on filamentous bacteriophages *fd* which have a contour length of 880 nm and a diameter of 6.6 nm.[4] There are two unique advantages of this particular system. First, each *fd* virus is essentially identical to all others, which results in suspensions of high monodispersity. This enables direct quantitative comparison with theory since it eliminates usual complications related to the polydispersity of rods.[5] In addition, monodisperse viruses easily form more complex phases such as a smectic liquid crystal.[6] Second, *fd* viruses have an aspect ratio that is larger than 100. Therefore, they satisfy the Onsager criterion which quantitatively describes the isotropic–nematic phase transition only for rods with the aspect ratio larger than 75.[7] For rods with smaller aspect ratios, the free energy expansion cannot be terminated at the second virial coefficient and must include third and higher order terms. These two features make *fd* a unique model system to quantitatively test the Onsager theory and its various extensions.

In an ideal system of rodlike molecules, one would have the ability to independently tune the microscopic parameters such as rod aspect ratio, flexibility, and molecular chirality. For filamentous viruses, a first step in this direction was accomplished by demonstrating that their aspect ratio can be continually tuned through standard molecular cloning techniques.[8,9] In contrast, the possibility of tuning the molecular chirality or flexibility of filamentous viruses remains unexplored. Here, we study the properties of *fd* Y21M, a virus which has a single point mutation in the amino-acid sequence of the major coat protein. In the first part of this report, we show that this simple change at the molecular level changes the persistence length of the virus by fourfold. For *fd wt*, the ratio of contour length to persistence length is 0.3, while for *fd* Y21M this ratio is closer to 0.1. We show that the isotropic–cholesteric phase transition of *fd* Y21M is described by the Onsager theory for perfectly rigid rods, in contrast to *fd wt*, where flexibility of the rods needs to be taken

Department of Physics, Brandeis University, Waltham, MA 02454, USA. E-mail: zdogic@brandeis.edu
† Electronic supplementary information (ESI) available: Videos S1–S4. See DOI: 10.1039/b822478a

into account. Our measurement of the isotropic–cholesteric phase coexistence in *fd* Y21M represents a first quantitative test of the Onsager theory. In addition, this work opens up the possibility of continually tuning the persistence length of *fd* virus by varying the ratio of the wild type and Y21M major coat protein in the final virus assemblage.

In the second part of the paper, we use the same mutant virus to investigate the microscopic origin of the cholesteric phase. Chirality of the constituent molecules at the microscopic level profoundly influences the properties and phase behavior of materials at macroscopic lenghtscales. Materials whose existence is a direct consequence of chirality include twist grain boundary (TGB) phases, various blue phases, the conical phase, and traditional cholesterics.[10–12] Notwithstanding the paramount importance of chirality, there is a missing connection between the microscopic chirality of the individual molecules and the macroscopic properties of entire chiral assemblages. For example, it remains a daunting challenge to predict the pitch of a cholesteric liquid crystal from a microscopic structure of the constituent molecules.[13,14] Hard rods by themselves are achiral molecules and it follows that they will form an achiral nematic phase. Straley was the first to extend studies of hard rods to chiral molecules, by analyzing the behavior of threaded rods.[15]

Experimentally, the chiral phase behavior of *fd* viruses and numerous other filamentous viruses has been investigated in great detail. All the viruses examined so far have a chiral microscopic structure. Therefore, one would expect that all the microscopically chiral viruses would form a cholesteric phase. However, this turns out not to be the case. Some viruses form a tightly wound cholesteric phase with a pitch that can be as small as ten microns, while other viruses form a nematic-like phase with no measurable twisting.[16,17] The exact microscopic chiral feature that causes some viruses to form cholesteric structures while other one to form nematic like phases remain unknown. A hypothesis has been put forward that assumes viruses in solution assume a helical superstructure and that mesoscopic interactions of helices results in the formation of a macroscopic cholesteric helix.[18] The formation of helices is thought to arise from incommensurate interactions between positively charged major coat proteins and negatively charged DNA.[17]

Here, we investigate the properties of the cholesteric phase of *fd* Y21M, and show that its cholesteric pitch is different by fivefold when compared to the pitch of *fd wt*. Furthermore, the handedness of the cholesteric twist switches from a left-handed helix for *fd wt* to right-handed for *fd* Y21M. Using mixtures of *fd wt* and *fd* Y21M, we create a system in which the precise control over the cholesteric twist is possible. These results greatly extend the potential of *fd* as a model lyotropic liquid crystalline material, and at the same time, allow us to correlate the existence of the cholesteric liquid crystalline phase with the persistence length of the virus and the presence of disorder in the packing of the virus coat protein.

2 Experimental methods

Filamentous virus *fd wt* is a long rodlike polyelectrolyte with a contour length of 880 nm and diameter of 6.6 nm. It consists of a cylindrical shell composed of approximately 2700 copies of the major coat protein pVIII which encapsulate a circular single stranded DNA.[19] The contour length of the virus is determined by the size of its DNA. The *fd wt* and *fd* Y21M differ only by a single point mutation in which the 21st amino acid of the major coat protein is changed from tyrosine (Y) to methionine (M). Using standard biological procedures, large quantities of the viruses were grown and purified using Xl1-Blue as a host *E. Coli.* strain.[20] We find that viruses grown with Xl1-Blue host are highly monodisperse. All samples were prepared in buffer at pH = 8.05 containing 100 mM NaCl and 20 mM Tris. Concentrations of the virus were determined using absorption spectroscopy. The optical density of *fd wt* for 1 mg/ml solution is $OD^{1\ cm}_{269\ nm} = 3.84$.[21] Equivalent absorbance for *fd* Y21M was calculated to be 3.63, accounting for the lack of absorption of methionine at 269 nm. To measure the persistence length, viruses were grown using a host strain JM101. These viruses were found to contain a significant number of multimers, some of which were up to ten microns long. Viruses were fluorescently labeled with Alexa-488 dye (Invitrogen, Eugene, OR), according to the previously published protocol.[22] A low volume fraction of these viruses was suspended in a solution of non-adsorbing polymer (20 mg/mL, Dextran MW 500 000) and placed between a coverslip and coverslide. Slides and coverslips were cleaned in 0.5% detergent solution (Hellmanex, Hellma, Plainview, NY) heated to 70 °C. Subsequently, the slides were immersed in 5 M NaOH, thoroughly rinsed, and then sonicated. Non-adsorbing polymers cause viruses to adsorb onto a glass surface due to the depletion interaction, effectively confining filaments to two dimensions, and ensuring they always remain in the focal plane. When the glass is properly cleaned, adsorbed viruses continue to fluctuate in 2D. Individual fluorescently labeled viruses were visualized using an inverted microscope (Nikon TE2000) equipped with a high numerical aperture oil objective (100X PlanFluor NA 1.3) and a Mercury Halide lamp (Excite-120). To reduce photobleaching effects a standard oxygen scavenging solution is added consisting of glucose oxidase (200 μg/ml), catalase (35 μg/ml) and glucose (4.5 mg/ml).[23] Images were collected with a high sensitivity CCD camera (Andor iXon 897) operating in a conventional mode. Exposure time was kept at minimum (less then 30 ms) in order to reduce blurring effects. Images were analyzed according to the previously published procedures.[23]

To characterize the behavior of the cholesteric phase, glass cylindrical capillaries, 0.7 mm in diameter (Charles Supper Company, Natick MA), were filled with samples of *fd wt* or *fd* Y21M. After equilibration, which can take up to a few days, these samples exhibit a well known fingerprint texture under polarization microscopy characteristic of a cholesteric liquid crystalline phase.[16] From such micrographs, it is easy to measure the cholesteric pitch, which is simply twice the distance between two neighboring peaks. In order for the cholesteric texture to properly develop, it was necessary to thoroughly clean the capillaries in a hot detergent solution (Hellmanex) after soaking in 5 M NaOH.

To further characterize the cholesteric phase, a second method was employed that is more sensitive for measuring large cholesteric pitches, and at the same time, elucidates the handedness of the cholesteric twist.[24] Liquid crystalline samples were confined between microscope slides and coverslips separated by 60 μm spacers of unstretched parafilm. The boundary conditions imposed by the glass surfaces ensure that twisting occurs along

a helical axis perpendicular to the image plane. Samples were doped with a low volume fraction of fluorescently labeled viruses, and a z-stack of images was acquired by changing the focal plane of the microscope (Fig. 2). Fluorescence microscopy reveals the orientation and anisotropic diffusion of individual labeled rods which coincides with the orientation of the local nematic director.[22] In order to image through thick samples, a water immersion objective with a long working distance was used for this part of the experiment (Nikon 60x NA 1.2). By determining how virus orientations change with z-position, we quantitatively measure the cholesteric pitch, and simultaneously determine its handedness. The second method based on fluorescence microscopy is particularly advantageous for investigating weakly twisted samples, where the length of the cholesteric pitch approaches the capillary diameter and boundary conditions suppress the formation of twisted structure. Measurements of cholesteric pitches larger than 1 mm can be made using this method. For samples where measurements were made using both capillary and florescence methods, equivalent results were found.

3 Results

3.1 Persistence length of *fd wt* and *fd* Y21M

We first measure the persistence length of *fd* Y21M by directly visualizing equilibrium conformations of individual freely fluctuating viruses. Due to a finite resolution of an optical microscope, a one micron long virus essentially appears as a straight rod and is therefore unsuitable for any quantitative analysis. For this reason, we analyzed the fluctuations at larger wavelengths easily observable in multimeric viruses. Multimeric viruses have the same structure as monomeric viruses and should yield the same value of the bending rigidity since this is a material property of the virus which is independent of its contour length. Fig. 1 shows typical conformations of *fd wt* and *fd* Y21M viruses. It is evident from these images that *fd wt* appears significantly more kinky when compared to *fd* Y21M (see also ESI,† videos 1 and 2), which indicates that the persistence length of *fd* Y21M is larger than *fd wt*. To quantitatively extract the persistence length from a sequence of images, a conformation of the virus is described by $\theta(s)$ where s is the position along the contour and θ is the local tangent angle. Local curvature of the rod is related to the derivative $d\theta(s)/ds$ and local elastic energy of a semiflexible filament is proportional to the square of the local curvature $(d\theta(s)/ds)^2$. The total energy of the filament with a conformation $\theta(s)$ is obtained by integrating along the contour length of the entire filament:

$$H = \frac{\kappa_b}{2}\int_0^L \left(\frac{d\theta(s)}{ds}\right)^2 ds \qquad (1)$$

Here κ_b is the bending rigidity of the filament and L is its contour length. The lowest energy state is that of a straight line which corresponds to $\theta(s) = \text{const}$. Next, $\theta(s)$ is decomposed into a Fourier series, $\theta(s) = \sum_q \sqrt{\frac{2}{L}} a_q \cos(qs)$ where $q = n\pi/L$ is the wavelength of the fourier mode and a_q is its amplitude. Combining this expression with eqn 1, one obtains that the energy of a filament deformed into a single fourier mode with amplitude a_q and wavelength q is given by $\frac{1}{2}\kappa_b a_q^2 q^2$. The total energy of any conformation is obtained by summing up over all the Fourier modes $H = \sum_q \frac{1}{2}\kappa_b a_q^2 q^2$. According to the equipartition theorem, each independent mode will have an average of $\frac{1}{2}\kappa_b T$ energy. It follows that the mean square value of each mode of wavelength q will be $\langle a_q^2 \rangle = \frac{k_b T}{q^2 \kappa_b}$. The bending rigidity is related to the persistence length as follows: $l_p = \kappa_b/k_b T$. We note that the fluctuations of each Fourier mode a_q yield an independent measurement of the persistence length.

We routinely collect a sequence of up to 5000 images, each revealing a distinct virus conformation. For each filament, $\theta(s)$ is obtained using previously published imaging procedures[23] and subsequently each conformation is decomposed into its Fourier components a_q. For each wavelength we measure $\langle (a_q - \langle a_q \rangle)^2 \rangle$ averaged over all the conformations. Fig. 2 shows experimentally measured fluctuation spectra $[\langle (a_q - \langle a_q \rangle)^2 \rangle$ vs $q]$ for both *fd wt* and *fd* Y21M. Experimentally we find that $\langle a_q \rangle$ is almost zero indicating that the lowest energy state is that of a straight rod. In the limit of low q, the fluctuation spectra scales as $1/q^2$. This confirms that the fluctuations of the viruses are properly described by the Hamiltonian in eqn 1. From this regime, we extract the bending rigidity of the filaments. In the limit of high q, fluctuations due to imaging noise dominate over physical fluctuations which have a small amplitude and therefore cannot be resolved with optical microscopy. Consequently the fluctuation spectrum flattens out. The details of how to correctly interpret the fluctuation spectrum are discussed in ref. 23. Analyzing the fluctuations of 24 different filaments we measure the persistence length of *fd wt* to be 2.8 ± 0.7 μm. We also analyzed fluctuations for 16 different *fd* Y21M viruses. Averaging this data, we measure the persistence length of the *fd* Y21M virus to be 9.9 ± 1.5 μm. At present it is unclear why a single point mutations in

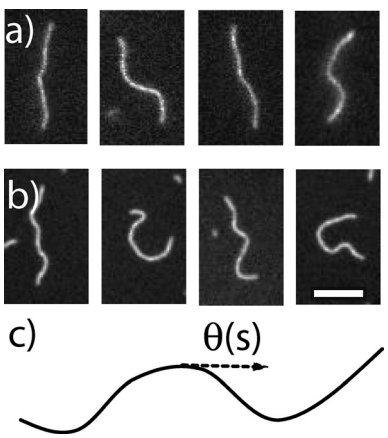

Fig. 1 Typical conformations of multimeric fluorescently labeled *fd wt* and *fd* Y21M viruses imaged with fluorescence microscopy. (a) A sequence of images illustrating independent conformations of a freely fluctuating *fd* Y21M virus confined to two dimensions. When analyzed these images yield the persistence length of 9.9 ± 1.6 μm. (b) Images of *fd wt* taken under same conditions. The persistence length of *fd wt* is determined to be 2.8 ± 0.7 μm. Scale bar is 5 μm. (see ESI,† videos 1 and 2) (c) A conformation of semiflexible filament is described by a function $\theta(s)$ where s represents the position along the contour length and θ is the orientation of the local tangent.

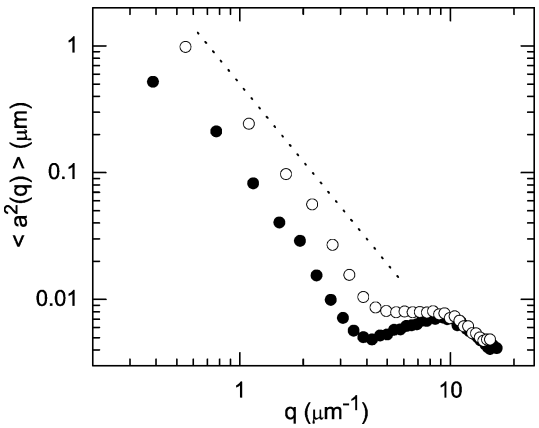

Fig. 2 A fluctuation spectrum of *fd wt* (○) and *fd* Y21M (●). At low wavenumbers the fluctuation spectrum scales as q^{-2} (indicated by dotted line) as is expected for wormlike chains. In this regime each point represents an independent measurement of the bending rigidity. To obtain the average persistence length we average over all points for which $q < 2\ \mu m^{-1}$. At high wavenumber, imaging noise dominates over physical fluctuations and the spectrum saturates at finite value.

the coat protein induces such a dramatic change in the persistence length. A possible explanation is related to recent observation that *fd* Y21M has significantly more order in packing of its major coat protein when compared to *fd wt*.[25,26] It seems reasonable that rods with more ordered internal structure should have higher persistence length. These findings are discussed in more detail in latter parts of the paper.

A number of different methods have been used to characterize the persistence length of *fd wt* and it is worthwhile to compare our results to previous measurements of the persistence length of *fd wt*. First, viruses have been directly dried on an electron microscopy (EM) grid and imaged using electron microscopy. These experiments yield a persistence length that ranges between 0.6 and 6 microns,[27] with the most recent study reporting the value of 1 μm.[25] The drawback of the EM methods is that preparation of EM grids involves a drying process which can easily alter the equilibrium conformations of soft filaments. In fact, one publication finds that the extracted persistence length significantly depends on the method used to prepare EM grids.[27] Second, dynamical light scattering was used to extract the persistence length of 2 microns.[28,29] Third, the persistence length of the virus was also extracted from force-extensions experiments,[30] and from the characteristics of the depletion potential that *fd* particles induce between micron sized polymer colloids.[31] Both of these methods yield a persistence length of approximately 1 μm. The disadvantage of the latter methods is their dependence on a particular model and require accurate knowledge of other parameters such as filament contour length. In comparison, the method described in this paper is the most direct measurement of the bending rigidity. It avoids any drying artifacts that accompany EM imaging and is essentially model independent. When interpreting fluctuation spectrum, it is important to distinguish regimes dominated by physical filament fluctuations from regimes in which measurement error dominate. The details of this procedure are discussed elsewhere.[23] Moreover, this method has been used to obtain reliable persistence lengths of other biopolymers such as actin and microtubules.[32] For these reasons, we believe that the value of 2.8 μm presents the most accurate measurement of the persistence length of *fd wt* obtained so far. We also note that in our previous work involving modeling of the phase behavior of *fd wt* we assumed the persistence length of *fd wt* to be 2.2 μm, a value which is very close to our new measurement.

3.2 Isotropic–cholesteric phase transition

Next, we examine the characteristics of the isotropic–cholesteric phase transitions for *fd* Y21M. We first note that although *fd* viruses form a cholesteric phase, the Onsager theory describing the isotropic–nematic phase transition is also valid for systems that undergo an isotropic–cholesteric phase transition. The free energy difference between the cholesteric and nematic phase is minimal and in this section we use terms cholesteric and nematic interchangeably.

To measure the concentration of coexisting phases, liquid crystalline samples are initially prepared within the isotropic–cholesteric coexistence region. Over a period of a few days the higher density nematic (cholesteric) phase sediments and bulk phase separation ensues. At this point, a sample is drawn from both coexisting phases and concentrations are determined using absorbance spectroscopy. For *fd* Y21M, we measure the concentration of coexisting isotropic and cholesteric phases to be 13.9 mg/ml and 18.9 mg/ml, respectively. In comparison, the coexistence concentrations for *fd wt* are found to be 19.8 mg/ml and 22.6 mg/ml in agreement with a previous report.[35] Because *fd wt* and *fd* Y21M are essentially identical to one another except for their flexibility, it is natural to assume that the difference in their phase behavior is due to their significantly different persistence lengths.

The influence of flexibility on the isotropic–nematic phase transition has been studied theoretically in great detail. As first demonstrated by Khokhlov and Semenov (KS), the flexibility of rods dramatically alters the nature of the isotropic–nematic phase transition.[3,33] In a nematic phase, fluctuations of semi-flexible filaments are severely constrained. This imposes an additional free energy penalty associated with the formation of a nematic phase, one that is not present for a suspension of perfectly rigid rods. It follows that the isotropic-nematic phase transition of semi-flexible rods is suppressed and occurs at higher particle densities when compared to a system of rigid rods. In the KS theory, the important parameter characterizing the semiflexible nature of the filaments is the ratio of contour length, L, to persistence length, p. Rods with $L/p < 0.1$ can be treated as effectively rigid and their behavior is described by the original Onsager theory. As L/p increases above a value of 0.1, the flexibility significantly influences the nature of the transition. For rods with $L/p \approx 0.5$ the location of the transition shifts to 30% higher densities when compared to rigid rods, the order parameter S of the coexisting nematic phase drops from $S \approx 0.8$ to $S \approx 0.6$, and the width of the coexistence region narrows from 30% to less than 10%.[33]

Filamentous viruses *fd* Y21M and *fd wt* are ideal model systems to test the predictions of the Onsager and KS theories respectively. The value of L/p for *fd wt* is 0.3, and therefore its phase transition should be described by the KS theory. In contrast, for *fd* Y21M, L/p is 0.1, and the phase transition in this

system should be described by the original Onsager theory for rigid rods. The isotropic–cholesteric phase transition for *fd wt* has been studied previously and in the limit of high ionic strength, the agreement with the KS theory is quantitative. In particular, it is found that the transition shifts to higher densities,[34,35] the order parameter at phase coexistence is significantly lower than the Onsager prediction,[36] and the coexistence region is much narrower.

Next, we compare the behavior of *fd* Y21M to the Osnager theory for rigid rods. The numerical solution of the Onsager theory yields the following concentrations for the coexisting isotropic, $c_{\text{iso}} = 3.289D/L$, and nematic phases, $c_{\text{nem}} = 4.192D/L$, where $c = \frac{\pi}{4} LD^2 \frac{N}{V}$, D is the diameter of the rod, L is the rod contour length and N/V is the number density.[5,37] To account for the electrostatic repulsion, we rescale the diameter according to the well established procedure originally introduced by Onsager.[1,35,38] For an ionic strength of 110 mM, an effective line charge of 1 e/Å, and a bare diameter of 6.6 nm this procedure yields $D_{\text{eff}} = 104$ Å. Translating these coexistence concentrations into experimental units, Onsager theory predicts coexistence concentration for *fd* Y21M rods of $\rho_{\text{iso}} = 14.2$ mg/ml and $\rho_{\text{nem}} = 18.1$ mg/ml. These predictions are remarkably close to our experimentally measured values of 13.9 mg/ml and 18.9 mg/ml.

Our results clearly demonstrate that at the level of the isotropic–nematic phase transition, *fd wt* behave as semiflexible rods, while *fd* Y21M approximate the behavior of rigid rods as described by the original Onsager theory. Despite its importance, until now there have been no direct and quantitative tests of the original Onsager theory for the isotropic–nematic phase transition of hard rods. As discussed above, Onsager theory fails to describe the phase behavior of *fd wt* due to its inherent flexibility. The isotropic–nematic phase transition has also been characterized for rod like Tobacco Mosaic Virus (TMV) particles.[39,40] However, Onsager theory fails to quantitatively describe the phase behavior of TMV systems. The aspect ratio of TMV particles is approximately 15, and the Onsager theory quantitatively fails for rods with an aspect ratio below 75. In most other systems, the particles are either too polydisperse and/or short to enable quantitative comparison with theory. For these reasons, our measurement of the isotropic–nematic phase coexistence for *fd* Y21M present a first quantitative test of the Onsager theory for rigid rods. We note that a more stringent test of the Onsager theory would be to measure the order parameter of the coexisting nematic phase.[36]

3.3 The cholesteric phase of *fd* Y21M and *fd* Y21M/*fd* mixtures

Increasing the concentration of rods beyond the isotropic to liquid crystal phase transition, *fd* viruses exhibit evidence of a twisted cholesteric phase. Here, we investigate the properties of cholesteric phase of *fd* Y21M and compare its behavior to *fd wt*, as well as discuss interesting behavior observed in mixtures of the two viruses.

Fig. 3a shows a characteristic cholesteric fingerprint texture of *fd wt*,[16] while Fig. 3b shows a similar pattern formed by *fd* Y21M for the same concentration of virus. It is immediately clear that

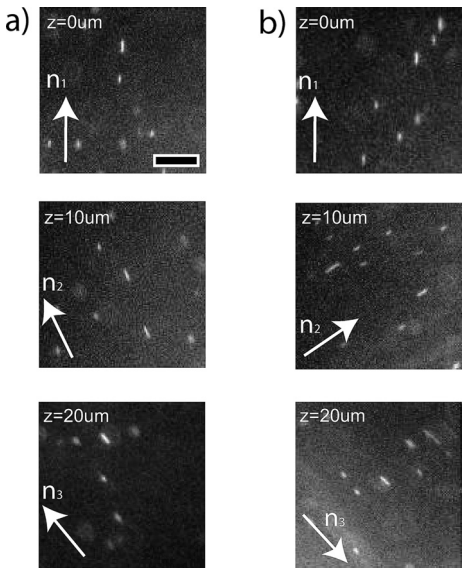

Fig. 4 Reconstruction of a cholesteric helix with fluorescence microscopy. A small volume fraction of fluorescently labeled rods reveals the orientation of the nematic director at a particular focal plane within the sample. Focusing into the sample, this director rotates in space tracing out a helix. This change in rotation for a given distance was used to measure the cholesteric pitch for a given sample. (a) A stack of images taken at different z-positions, spaced 10 μm apart, for a cholesteric liquid crystalline sample of *fd* Y21M. (b) Equivalent stack taken for cholesteric phase of *fd* wt. Both *fd* Y21M and *fd wt* samples at prepared at 50 mg/ml. The difference in both the handedness and the magnitude of the twist is self-evident. To determine the handedness, it is necessary to take into account the mirrors along the optical path of the microscope, which invert the chirality of the actual helix. The images shown are what is observed on the camera, and are the opposite handedness of the true handedness because of the odd number of mirrors present in the optical path of the microscope. Scale bars are 5 microns. (See ESI,† videos 3 and 4.)

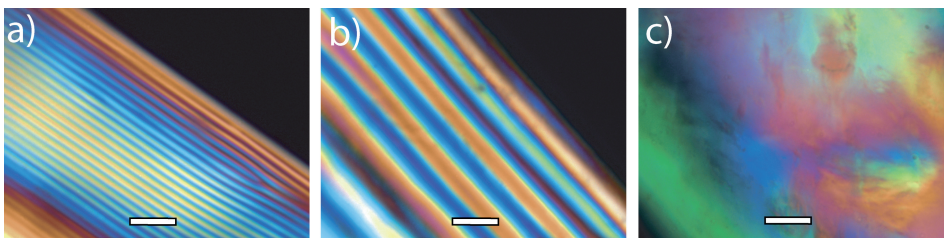

Fig. 3 Polarization micrographs of liquid crystalline samples of (a) pure *fd wt*, (b) pure *fd* Y21M and (c) mixture of 20% *fd wt* and 80% *fd* Y21M. Concentrations of the viruses in all the samples is fixed at 80 mg/ml. The characteristic fingerprint texture shown in (a) and (b) is indicative of a chiral cholesteric phase. The ratio of measured cholesteric pitches, *fd wt* to *fd* Y21M, at this concentration was 0.21. When a mixture of the viruses is prepared near this same ratio, no signs of chiral cholesteric ordering are observed in panel (c). All scale bars are 50 μm.

the properties of these cholesteric phases are dramatically different, with *fd* Y21M having a much larger cholesteric pitch. This is surprising considering that the difference between the *fd wt* and *fd* Y21M is in a single amino acid of the major coat protein pVIII. Even more striking, is the behavior of mixtures of the two viruses. Fig. 3c shows a sample which contains 20% *fd wt* and 80% *fd* Y21M. All samples mixed at or near these ratios exhibit similar behavior: no visible cholesteric patterns. Qualitatively, this implies the formation of a cholesteric phase with a pitch that is larger then the capillary diameter. To investigate this further, we reconstruct the cholesteric helix by directly visualizing the nematic director using the procedure described in the experimental methods section (Fig. 4). We find that *fd wt* forms a left-handed helix, while *fd* Y21M forms a right-handed helix. This observation explains why a mixture of *fd wt* and *fd* Y21M viruses form a nematic like phase with no measurable twisting effects, with the oppositely handed twist canceling each other.[10]

Next, we quantify these observations on the cholesteric phase of *fd wt* and *fd* Y21M. The cholesteric pitch as a function of virus concentration is plotted for both the *fd wt* and *fd* Y21M in Fig. 5. Previously published reports showed that the cholesteric pitch, P, of *fd wt* scales with virus concentration according to the expression $P \propto c^{\alpha}$.[16] For *fd wt* we find a value of $\alpha_{wt} = -1.6 \pm 0.08$, in agreement with previously published data. The dependence of the cholesteric pitch on concentration for *fd* Y21M also fits to a power law behavior with an exponent of $\alpha_{Y21M} = -1.9 \pm 0.2$. Within experimental uncertainties, these exponents are almost indistinguishable, and for samples at the same virus concentration, the cholesteric pitch of *fd wt* is approximately five times smaller than *fd* Y21M.

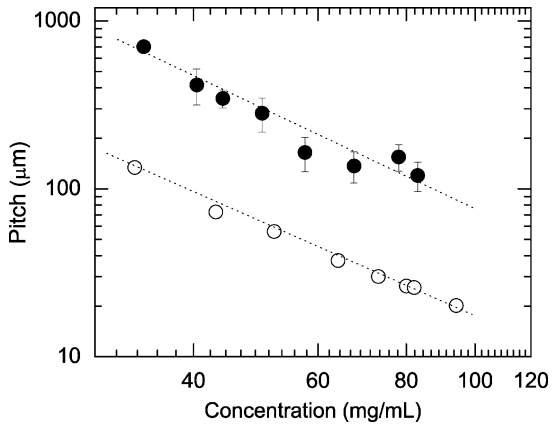

Fig. 5 Log–log plot of the cholesteric pitch of both *fd wt* (○) and *fd* Y21M (●) as a function of the virus concentrations, c. For both samples, cholesteric pitch, P, scales as $P \propto c^{\alpha}$. This scaling is indicated with a dotted line.

As already demonstrated in Fig. 4c, having two viruses with opposite helicity, which are very similar to each other, opens up the possibility of creating mixed systems in which the macroscopic chiral properties of the overall mixture can be precisely tuned by controlling the ratio of *fd wt* and *fd* Y21M. Mixtures in which the ratio of *fd wt* and *fd* Y21M was systematically varied were prepared at a fixed overall concentrations of either 55 mg/ml or 80 mg/ml. The behavior of the cholesteric pitch in these mixed systems is illustrated in Fig. 6. As the ratio changes from 1 (corresponding to a pure *fd wt* sample) to 0.4, where 40% of the particles are *fd wt*, the cholesteric pitch is left-handed and increases in magnitude with decreasing ratio. Below a ratio of 0.4, the cholesteric pitch continues to increase and becomes extremely large, until the onset of nematic like ordering with no measurable twisting occurs at a ratio of approximately 0.2. We note that for samples with a cholesteric pitch larger than 1 mm, it becomes increasingly difficult to accurately determine its magnitude due to local distortions of the nematic director caused by topological defects. Hence, there are large error bars. Decreasing the ratio of *fd* wild-type to Y21M even further, a right-handed cholesteric pitch is recovered.

Colloidal rodlike particles in which excluded volume interactions dominate the phase behavior offer a unique system in which it might be possible to establish a rigorous connection between microscopic chirality of individual molecules and macroscopic chirality as exhibited in the cholesteric phase. However, despite intensive efforts, the microscopic origin of the cholesteric twist still remains poorly understood. The first study in this area has shown

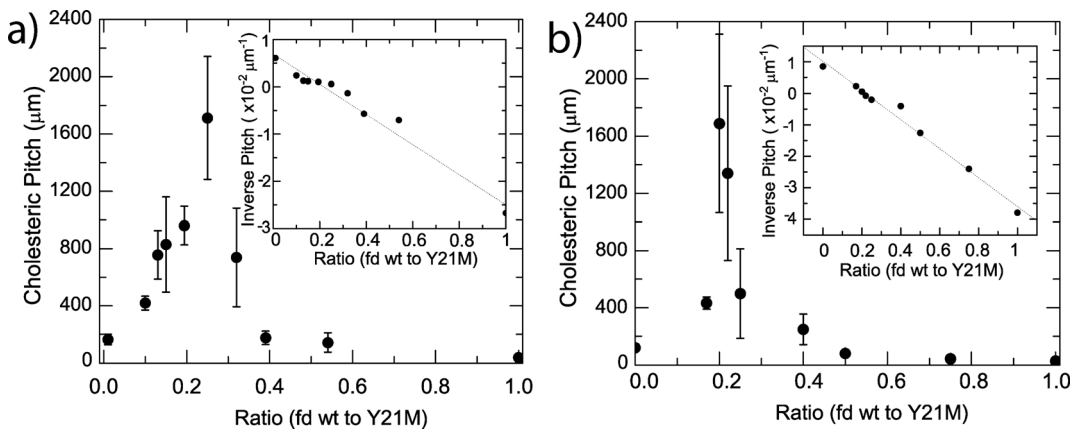

Fig. 6 Plots of the cholesteric pitch for samples in which the ratio of *fd wt* to *fd* Y21M is varied while total virus concentration is held constant at (a) 55 mg/ml and (b) 80 mg/ml. The cholesteric pitch is shown to be systematically tunable using different mixture ratios of the two viruses. At a mixing ratio of approximately 0.2, the samples exhibit no measurable twisting effects, indicating a nematic like structure. Insets: assigning positive and negative values to right- and left-handed pitches respectively, the inverse pitch is plotted for the different ratios of viruses. These behave roughly linear for both cases.

that *fd wt* virus forms a cholesteric liquid crystal, while *Pf1*, a virus with a similar structure and microscopic chirality, forms a nematic liquid crystal.[16] Subsequent studies showed that the cholesteric phase of *fd wt* persists even when viruses are coated with an achiral polymer brush which presumably screens any chiral interactions at the molecular level.[18] A hypothesis was put forward that *fd wt* in solution assumes a shape of a supramolecular helix. Helices differ from rod-like particles in that they minimize excluded volume by approaching each other at a slight angle.[15] Recently, a mechanism by which the supramolecular helix arises in some bacteriophages has been proposed.[17] In this important study, a diverse group of filamentous viruses were investigated: some were found to form cholesteric phases while others form nematic phases. It was proposed that the interactions between a negatively charged DNA and positively charged coat proteins induce internal strain which leads to the formation of a supramolecular helix. This hypothesis is supported by the observation that the addition of silver ions, which disrupt the DNA-protein interactions, changes the pitch of the cholesteric phase. These important experiments point towards a method in which the microscopic chirality of viruses can be continuously tuned through chemistry. An alternative proposal relates the properties of the cholesteric phase to the the exact helical distribution of charges along the surface of the virus.[24] This work explains how viruses with a right-handed helical charge distribution form a left-handed cholesteric helix. A stringent test of this theory would be to take the helical distribution of charge in *fd* Y21M and see if this changes the handedness of the resulting cholesteric helix.

Simultaneous with liquid crystalline studies of filamentous viruses a great deal of insight has been gained about the microscopic structure of individual viruses. Each virus consists of a cylindrical shell in which approximately 2700 major coat proteins (pVIII) pack on a regular lattice. This cylindrical shell encloses a single stranded DNA which carries of the information required for virus replication. NMR studies have shown that the order associated with packing of pVIII in *fd wt* increases with increasing temperature, and that the structure of *fd wt* at high temperatures is similar to the Y21M mutant at room temperature.[26] In other words packing of the coat protein in *fd* Y21M is much more regular when compared to *fd wt*. These conclusions are also supported by recent high resolution electron microscopy reconstruction of *fd wt* and *fd* Y21M structure.[25] Based on the analysis of X-ray diffraction patterns, it has been proposed that Tyrosine(Tyr) at 21 position of the amino acid sequence from one pVIII protein forms a hydrogen bond with a Tryptophan 26 in the neighboring pVIII protein.[41,42] Mutating Tyrosine into Methionine suppresses the formation of this hydrogen bond. The mechanism by which a suppression of a single hydrogen bond leads to dramatic changes in the flexibility of the virus and their ability to form a twisted nematic phase remains unclear.

Our study points towards a tentative connection between the twist of the cholesteric phase and the disorder present in the packing of the major coat protein pVIII within each rodlike virus. At a macroscopic liquid crystalline level, we have already shown that the cholesteric pitch unwinds with increasing temperature.[16] In this paper, we demonstrate that *fd* Y21M, a mutant with increased order, forms a cholesteric phase with an anomalously large pitch. At a microscopic level, both *fd* Y21M and *fd wt* at elevated temperature exhibit increased order in the packing of the major coat protein when compared to *fd wt* at room temperature. From these observations, we can correlate the presence of disorder in the virus coat protein with more tightly wound cholesteric phases. These results seem consistent with the hypothesis put forward in ref. 17 that large scale chirality of viruses arises from a supramolecular helical structure. It seems plausible that larger internal strain in viruses arising from DNA-protein mismatches leads to a more pronounced helical conformation, which in turn leads to tighter cholesteric pitches, and, at the same time, increases the disorder present in packing of the major coat protein. Alternatively it is possible that increased disorder in the coat protein packing is correlated with the increased flexibility of the virus. Viruses with larger flexibility will require less energy to distort into a helical structure. What remains unclear is why a single point mutations induces the helicity to switch from a left-handed helix to a right-handed one.

It remains an important challenge for future studies to directly visualize the hypothesized large scale helical conformations of *fd wt* and *fd* Y21M in solution. At the same time, it is a challenge that offers a great opportunity to better our understanding of exactly how chirality at microscopic length scales can influence and dictate macroscopic chiral behavior. Visualizing the proposed helical structure of *fd* will enable rigorous test of theories that relate the microscopic helicity with the twisting of the cholesteric phase.

4 Conclusions

In conclusion, we find that *fd* Y21M exhibits significantly different macroscopic phase behavior when compared to *fd wt* despite the only difference on a microscopic level being a single amino acid of the major coat protein. We demonstrate that *fd* Y21M is a model system of rigid rods, and as such can be used to quantitatively test the Onsager theory. We have also shown that through specific genetic modification it is possible to tune the microscopic chirality and have demonstrated how this microscopic modification alters the macroscopic behavior of one of the simplest chiral structures: the cholesteric liquid crystal. These results enable us to correlate the increased twist of the cholesteric phase with increased disorder of the protein coat structure. These results form an essential stepping stone that will enable future studies seeking to correlate microscopic chirality of the viruses to the macroscopic structure of various chiral assemblages.[43] Our results also pave the way for construction of hybrid viruses that contain a known ratio of major coat proteins derived from *fd wt* and *fd* Y21M, with the flexibility and chirality of these hybrid viruses possibly spanning the two limits set by the values of *fd wt* and *fd* Y21M. This would create a powerful model system of semiflexible filaments with tunable persistence length and chirality. These would be of tremendous importance for investigating how microscopic features of the constituent particles affect macroscopic properties of their liquid crystalline assemblages.

Acknowledgments

This work was supported by NSF through grants DMR-0705855 and MRSEC-0820492, and the co-sponsored HHMI/NIBIB Quantitative Biology Program at Brandeis University. We thank Dr Stanley Opella for the generous gift of *fd* Y21M.

References

1 L. Onsager, *Ann. N.Y. Acad. of Sci.*, 1949, **51**, 627–659.
2 G. J. Vroege and H. N. W. Lekkekerker, *Rep. Prog. Phys.*, 1992, **55**, 1241.
3 A. R. Khokhlov and A. N. Semenov, *Physica A*, 1981, **108**, 546.
4 Z. Dogic and S. Fraden, *Curr. Opin. Colloid Interface Sci.*, 2006, **11**, 47–55.
5 H. N. W. Lekkerkerker, P. Coulon, R. van der Haegen and R. Deblieck, *J. Chem. Phys.*, 1984, **80**, 3427.
6 Z. Dogic and S. Fraden, *Phys. Rev. Lett.*, 1997, **78**, 2417.
7 D. Frenkel, *J. Chem. Phys.*, 1988, **92**, 3280.
8 J. F. Maguire, J. P. McTague and F. Rondelez, *Phys. Rev. Lett.*, 1980, **45**, 1891.
9 Z. Dogic and S. Fraden, *Phil. Trans. R. Soc. Lond. A*, 2001, **359**, 997.
10 P. G. deGennes and J. Prost, *The Physics of Liquid Crystals*, Oxford University Press, Oxford, U.K., 1995.
11 S. R. Renn and T. C. Lubensky, *Phys. Rev. A*, 1988, **38**, 2132.
12 E. Barry, Z. Hensel, Z. Dogic, M. Shribak and R. Oldenbourg, *Phys. Rev. Lett.*, 2006, **96**, 018305.
13 A. B. Harris, R. D. Kamien and T. C. Lubensky, *Phys. Rev. Lett.*, 1997, **78**, 2867.
14 A. B. Harris, R. D. Kamien and T. C. Lubensky, *Rev. Mod. Phys.*, 1999, **71**, 1745.
15 J. P. Straley, *Phys. Rev. A*, 1976, **14**, 1835.
16 Z. Dogic and S. Fraden, *Langmuir*, 2000, **16**, 7820.
17 S. Tomar, M. M. Green and L. A. Day, *J. Am. Chem. Soc.*, 2007, **129**, 3367.
18 E. Grelet and S. Fraden, *Phys. Rev. Lett.*, 2003, **90**, 198302.
19 L. A. Day, C. J. Marzec, S. A. Reisberg and A. Casadevall, *Annu. Rev. Biophys. Chem.*, 1988, **17**, 509.
20 *Molecular Cloning*, ed. T. Maniatis, J. Sambrook and E. Fritsch, Cold Spring Harbor Univ. Press, 1989.
21 S. Fraden in *Observtion, Prediction and Simulation of Phase Transitions in Complex Fluids*, ed. M. Baus, L. F. Rull, J. P. Ryckaert, Kluwer Academic Publishers, Dordrecht, 1995, 113–164.
22 M. P. Lettinga, E. Barry and Z. Dogic, *Europhys. Lett.*, 2005, **71**, 692.
23 C. P. Brangwynne, G. H. Koenderink, E. Barry, Z. Dogic, F. C. MacKintosh and D. A. Weitz, *Biophys. J.*, 2007, **93**, 346.
24 F. Tombolato, A. Ferrarini and E. Grelet, *Phys. Rev. Lett*, 2006, **96**, 258302.
25 Y. A. Wang, X. O. Yu, S. Overman, M. Tsuboi, G. J. Thomas and E. H. Egelman, *J. Mol. Biol.*, 2006, **361**, 209.
26 W. M. Tan, R. Jelinek, S. J. Opella, P. Malik, T. D. Terry and R. N. Perham, *J. Mol. Biol.*, 1999, **286**, 787.
27 K. Beck and R. M. Duenkim, *J. Struc. Biol.*, 1990, **105**, 22.
28 L. Song, U. Kim, J. Wilcoxon and M. Schurr, *Biopolymers*, 1991, **31**, 547.
29 T. Maeda and S. Fujime, *Macromolecules*, 1985, **18**, 2430.
30 A. S. Khalil, J. M. Ferrer, R. R. Brau, S. T. Kottmann, C. J. Noran, M. J. Lang and A. M. Belcher, *Proc. Nat. Acad. Sci.*, 2007, **104**, 4892.
31 A. W. C. Lau, K. H. Lin and A. G. Yodh, *Phys. Rev. E*, 2002, **66**, 020401.
32 F. Gittes, B. Mickey, J. Nettleton and J. Howard, *J. Cell. Biol.*, 1993, **120**, 923.
33 Z. Y. Chen, *Macromolecues*, 1993, **26**, 3419.
34 K. R. Purdy and S. Fraden, *Phys. Rev. E*, 2004, **70**, 061703.
35 J. X. Tang and S. Fraden, *Liquid Crystals*, 1995, **19**, 459.
36 K. R. Purdy, Z. Dogic, S. Fraden, A. Ruhm, L. Lurio and S. G. J. Mochrie, *Phys. Rev. E*, 2003, **67**, 031708.
37 J. Herzfeld, A. E. Berger and J. W. Wingate, *Macromolecules*, 1984, **17**, 1718.
38 A. Stroobants, H. N. W. Lekkerkerker and T. Odijk, *Macromolecules*, 1986, **19**, 2232.
39 R. Oldenbourg, X. Wen, R. B. Meyer and D. L. D. Caspar, *Phys. Rev. Lett.*, 1988, **61**, 1851.
40 S. Fraden, G. Maret, D. L. D. Caspar and R. B. Meyer, *Phys. Rev. Lett.*, 1989, **63**, 2068.
41 D. A. Marvin, R. D. Hale and C. Nave, *J. Mol. Biol.*, 1994, **235**, 260.
42 L. C. Welsh, M. F. Symmons, C. Nave, R. N. Perham, E. A. Marseglia and D. A. Marvin, *Macromolecules*, 1996, **29**, 7075.
43 E. Barry, Z. Dogic, R. B. Meyer, R. P. Pelcovits and R. Oldenbourg, *J. Phys. Chem. B*, 2009, **113**, 3910.

